Journal of Photochemistry and Photobiology A: Chemistry 224 (2011) 71–79

Contents lists available at SciVerse ScienceDirect

Journal of Photochemistry and Photobiology A: Chemistry

journal homepage: www.elsevier.com/locate/jphotochem

Influence of geometric and electronic characteristics of TiO_2 electrodes with nanotubular array on their photocatalytic efficiencies

A. Atyaoui[a,b,c], L. Bousselmi[a], H. Cachet[b,c], Peng Pu[b,c], E.M.M. Sutter[b,c,*]

[a] Laboratoire de Traitement des Eaux Usées, Centre de Recherches et Technologies des Eaux, BP. 273 8020 Soliman, Tunisia
[b] LISE, UPR 15 du CNRS, Université Pierre et Marie Curie, Case 133, 4 Place Jussieu, 75252 Paris Cedex 05, France
[c] University Pierre et Marie Curie, 4 place Jussieu, 75252 Paris Cedex 05, France

ARTICLE INFO

Article history:
Received 2 July 2011
Received in revised form 30 August 2011
Accepted 10 September 2011
Available online 20 September 2011

Keywords:
Titanium oxide
Nanotubes
Photocatalysis
Photocurrent
Impedance

ABSTRACT

The present work compares the efficiencies of titania nanotubes (NT) formed by anodizing of titanium at 20 V for 45 min in three kinds of electrolytes: ethylene glycol–ammonium fluoride–water (NT_1), tetrabutylammonium fluoride–formamide–water (NT_2) and sodium sulfate–ammonium fluoride–water (NT_3). The geometric characteristics were investigated by scanning electron microscopy (SEM). The photoactivities of the three layers were compared through photo-potential, photo-current measurements in an alkaline medium and in the presence of methanol as a hole scavenger. Impedance spectrometry was used for investigation of conduction and charge storage properties of the titania layer. Finally the photocatalytic properties were compared through the degradation rate of an azo dye, such as Amido Black (AB).

In comparison to NT_2 and NT_3, the NT_1 layer showed not only the highest photopotential, but also the highest photocurrent response. Photocatalytic results showed that the degradation of dye proceeds much faster in the presence of NT_1 as compared with other TiO_2 nanotube samples. Nevertheless photoinduced surface states were found to be more important in NT_2, in comparison with the two other layers. All these results are discussed taking into account the geometric characteristics of the nanotubular layers, not only the specific surface on one hand, but also the solid fraction of the external surface, which determines the level of light absorption able to generate photo-charges.

1. Introduction

TiO_2 is a widely used photocatalyst for degradation of organic pollutants in waste water, because of its high photosensitivity, long-term stability and non-toxicity [1]. The photocatalytic properties of TiO_2 nanotubular thin layers (NT) have been studied by several groups, and much higher decomposition efficiency than for a Degussa P25 nanostructured layer under similar conditions has been reported [2–4]. Two key factors influence the photocatalytic efficiency: the first one is the huge specific area of the nanotubular layer which allows increased adsorption of organic molecules during the photocatalytic reaction [4]. The second determining factor is the transport rate of the photogenerated charges through the layer. Nanotubular films made of oriented one-dimensional structures aligned perpendicular to the substrate are assumed to show improved charge-collection efficiency by promoting faster charge transport and slower recombination [5–8]. In nanostructured layers, the interfacial kinetics are also drastically affected by the presence of electron traps in the layer, and the charge transport in such films can be controlled by the mechanism of trapping–detrapping [9–18].

Among the different fabrication methods of NT, the titanium anodization method in fluoride-based baths provides good mechanical adhesion and good electronic conductivity, since it directly grows from the titanium metal substrate [2,19–24].

The thickness and morphology of such TiO_2 film are strongly affected by the electrochemical conditions (anodization voltage, duration of anodization, . . .) and the composition of the electrolyte (fluoride concentration, pH, water content in the electrolyte and presence of an organic solvent, . . .). Since the as-prepared samples show an amorphous structure, post-treatments are necessary to control the crystallinity of the nanotubes. Thermal annealing in the 450–600 °C temperature range is usually carried out to get a well crystallized anatase structure. Yu and Wang [25] showed that the calcinations temperature exhibits a great influence on the photocatalytic activity. A vapour-thermal treatment at 180 °C instead of calcination [26], or a chemical treatment of the tube walls applied after calcinations [27] has been shown to further improve the photocatalytic activity.

* Corresponding author at: LISE, UPR 15 du CNRS, Université Pierre et Marie Curie, Case 133, 4 Place Jussieu, 75252 Paris Cedex 05, France. Tel.: +33 1 44 27 41 68; fax: +33 1 44 27 40 74.
E-mail address: eliane.sutter@upmc.fr (E.M.M. Sutter).

1010-6030/$ – see front matter © 2011 Elsevier B.V. All rights reserved.
doi:10.1016/j.jphotochem.2011.09.009

Comparison between the morphology and the properties of nanotubular TiO_2 layers obtained in different electrolytes has been reported by Zlamal et al. [28]. They suggest that thick tube walls are needed for good catalytic performance since they allow more efficient separation of electron–hole pairs. Smooth tube walls are also beneficial for an improved electron diffusion length in the layer [5]. The presence of a high density of deep localized electronic states in the gap of nanotubular TiO_2 layers has been evidenced in [23], but no clear correlation between the presence of electronic states or traps, and the photocatalytic activity of the layer has been reported.

The aim of the present work is thus to contribute to establish a correlation between the morphology of the NT layers, the density of surface states present in the layers and their photocatalytic activity. Three kinds of NT layers with similar thicknesses were synthesized. The first kind of nanotubes (NT_1) was grown in ethylene glycol in order to get tubes with smooth walls. The second kind (NT_2) was obtained in a tetrabutylammonium fluoride solution prepared in formamide in order to get rough walls. The third kind of NT was synthesized in an aqueous medium in the absence of any organic solvent. The photoactivity of the three layers was compared through photo-potential and photo-current measurements. Impedance spectrometry was also used for investigation of conduction and charge accumulation properties. All the electrochemical experiments were performed in an alkaline medium and in the presence of methanol as a hole scavenger. Finally the photocatalytic properties were compared through the degradation rate of an azo dye, such as Amido Black (AB).

2. Experimental

2.1. Synthesis of TiO_2 nanotubular layers

Anodization was carried out at 20 V for 45 min, at room temperature using a DC power source in a two-electrode cell, where a Pt foil served as the counter electrode and a titanium sheet was used as the working electrode. Prior to anodization, the titanium foil was first mechanically polished with different abrasive papers, sonicated in acetone, ethanol and deionized (DI) water, and then dried in a N_2 stream.

Three kinds of TiO_2 nanotube arrays films were made by anodic oxidation of a titanium rod (2 mm thickness, 15 mm diameter, 99.6% purity) in the following solutions:

- for NT_1: ethylene glycol containing 3 wt% NH_4F and 2 vol% H_2O [29];
- for NT_2: 0.27 mol/L tetrabutylammonium fluoride solution prepared in formamide containing 3% deionized water [30,31];
- for NT_3: 1 mol/L Na_2SO_4 with 1 wt% NH_4F in water [32].

Finally, as-anodized samples were first thoroughly rinsed with ethanol and with water, dried under nitrogen then annealed in air at 500 °C during 2 h with a ramp-up and ramp-down rate of 1 °C/min.

2.2. Crystalline structure of the electrodes

The crystalline structures of the annealed electrodes were studied using an OLYMPUS-JOBIN YVON-Raman spectrometer. The surface morphology of films was observed using a scanning electron microscope SEM-FEG Ultra 55.

2.3. Photoelectrochemical procedure

Photoelectrochemical characterization was performed using a VoltaLab 40 PGZ301 potentiostat (Radiometer Analytical), connected with a computer that uses VoltaMaster 4.0 software for data acquisition. A 100 mL cell made of quartz was used as photoelectrochemical cell with the TiO_2/Ti electrode as working electrode, a Pt counter-electrode and a saturated calomel reference electrode (SCE). All potentials are quoted versus SCE. The geometric surface of the working electrode was 0.64 cm^2. The electrolyte was an air-saturated aqueous solution with 0.1 mol/L NaOH, with and without methanol. A 150 W Xenon lamp was employed as excitation source. The electrochemical investigations were performed in the dark and under light excitation in solutions containing different methanol concentrations (0–100 mmol L). Electrochemical impedance spectroscopy (EIS) measurements were carried out at the open-circuit potential. A sinusoidal AC perturbation of 10 mV was applied to the electrodes over the frequency range of 20,000–0.1 Hz. The experimental data from EIS diagrams were analysed using the software, ZsimpWin3.2.

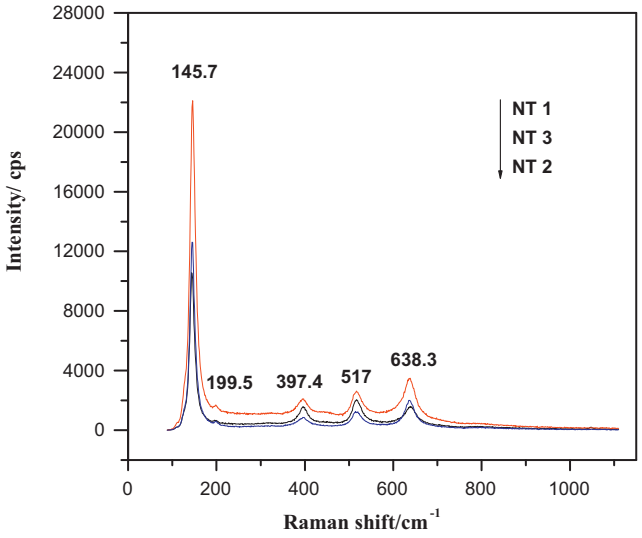

Fig. 1. Raman spectra for the three nanotubular TiO_2 layers.

3. Results and discussion

3.1. Raman spectroscopy analyses

Raman spectroscopy is a technique that can clearly identify the crystal forms of titania (anatase, rutile and brookite) even at very low levels. In fact the Raman spectrum of anatase single crystal shows six Raman bands at 144 (E_g), 197 (E_g), 399 (B_{1g}), 513 (A_{1g}), 519 (B_{1g}) and 639 cm^{-1} (E_g) [33]. The rutile phase is characterized by four Raman active modes at 143 (B_{1g}), 447 (E_g), 612 (A_{1g}), and 826 cm^{-1} (B_{2g}) [34]. The brookite phase has three Raman bands at 247, 326 and 366 cm^{-1} [35]. In this work, the Raman spectra of the three titania nanotubes samples mainly show the typical bands of anatase phase (see Fig. 1).

3.2. SEM analysis

Fig. 2 shows a typical SEM image of a TiO_2 nanotube layer prepared by anodization of titanium at 20 V for 45 min in the three different electrolytes. It can be seen from the top-view images that the nanotube array produced using ethylene glycol (NT_1) is more uniform, with smooth tube walls, well-oriented over the substrate. NT_2 tubes obtained in tetrabutylammonium fluoride and formamide solution show rough walls and the individual tubes are connected with each other via rings at the side walls. NT_3 tubes formed in aqueous medium in the absence of organic solvent are more spaced from each other in comparison with NT_1 and NT_2. They

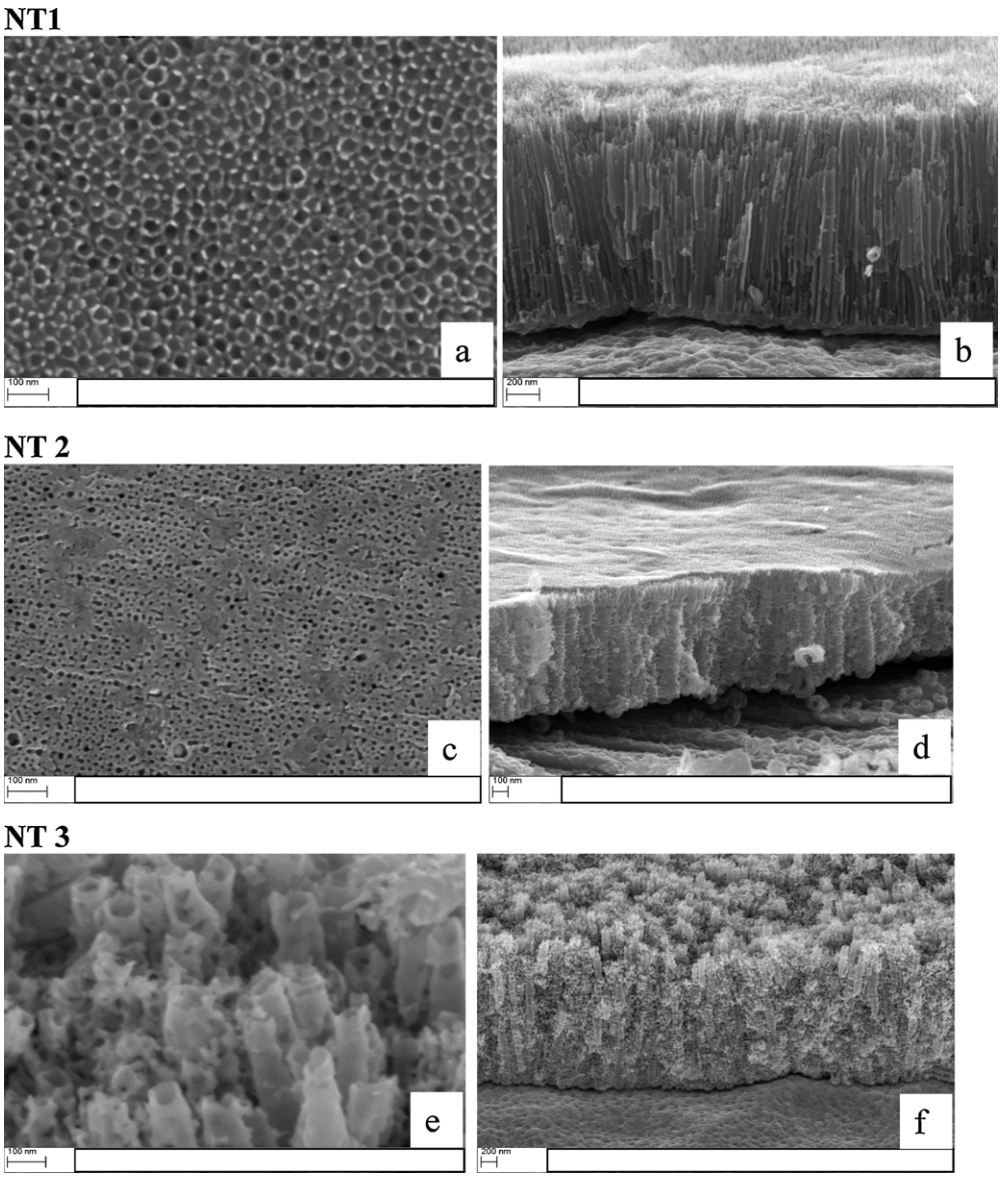

Fig. 2. SEM images of TiO_2 nanotubes layers formed on Ti substrate: (a, c and e) top-view; (b, d and f) cross-section of NT_1, NT_2 and NT_3, respectively.

seem less well-oriented over the substrate and the diameter of the tubes increases from top to the bottom of the layer. It is also clear from these pictures that for the three types of layers, the tubes are open on the top and closed at the bottom of the layer.

3.3. Geometric characteristics of the layers

The mean geometric parameters of the tubes: length (L), outer (D_{out}) and inner (D_{in}) diameter, wall thickness (w), void thickness (y) between the tubes are reported in Table 1. It is noticeable that the wall thickness (w) has similar values in the three layers.

According to [30,36], a geometric model with a regular network of identical and equally spaced nanotubes can be used for the estimation of the geometric roughness factor H, defined as the ratio of the cylindrical inner and outer surfaces relative to the corresponding projected area.

Considering the parameters L, y, and $R_1 = (1/2)D_{int}$; $R_2 = R_1 + (1/2)w$, the H factor is calculated as following:

$$H = \frac{8\pi L R_2}{\sqrt{3}(4R_2 - 2R_1 + y)^2} \quad (1)$$

The calculated geometric factor H and the corresponding specific surface ($S_{spec} = H \times$ geometric surface) are also reported in Table 1. Though NT_3 shows a higher tube length and a higher void thickness between the tubes, the specific area are of the same order of magnitude in the three layers, with a value slightly larger for NT_1.

Moreover, using the same geometric model the tube density is given by:

$$d_{NT} = \frac{2}{\sqrt{3}(4R_2 - 2R_1 + y)^2} \quad (2)$$

The solid fraction $S_\%$ is the surface ratio at the top of the layer able to absorb incident photons and is calculated according to Eq. (3):

$$S_\% = \frac{\pi}{4}({D_{out}}^2 - {D_{in}}^2)d_{NT} \quad (3)$$

The d_{NT} and $S_\%$ values are also reported in Table 1.

3.4. Open-circuit potential (E_{OCP})

Fig. 3(a) shows the evolution of the open-circuit potential with the concentration of methanol, in a 0.1 mol/L air-saturated NaOH

Table 1
Geometric parameters of the 3 layers with nanotube arrays (geometric surface = 0.64 cm^2). L: tube length; D_{in}: inner diameter; D_{out}: outer diameter; y: void thickness; w: wall thickness.

Electrode	L (nm)	D_{in} (nm)	D_{out} (nm)	y (nm)	w (nm)	H	Specific surface (cm^2)	d_{NT} cm^{-2}	$S_{\%}$
NT_1	1250	40	70	20	15	61	39	1.4×10^{10}	0.36
NT_2	800	23	63	20	20	36	23	1.7×10^{10}	0.47
NT_3	1700	70	106	50	18	45	29	0.47×10^{10}	0.23

solution, in the dark and under illumination. The values were taken when the steady state was reached, after 30 min of immersion.

In the absence of UV light, the OCP value is slightly more negative for NT_1 (−0.55 V) than for NT_2 (−0.50 V) and NT_3 (−0.52 V). In the three cases, it is independent of the concentration of methanol. On the contrary, under illumination, a clear shift of the OCP towards more negative values is observed, when the concentration of methanol, is increased, reaching a value of −1.05 V for NT_1 in 100 mmol L of methanol. Fig. 3(b) shows the variation of photopotential (difference between OCP in the dark and OCP under lightening) as a function of methanol concentration. It is noticeable that NT_1 shows the highest photo-induced potential shift among the three nanolayers.

Under open-circuit conditions, the photoanodic current must be associated with a cathodic reaction draining the photogenerated electrons. The increase of the photopotential with increasing methanol concentration can thus be attributed to the increase of the anodic reaction (hole consumption by methanol), when methanol concentration increases. Simultaneously, more electrons are available to accumulate in the electrode. Comparing the photopotential values in the three types of layers, we must admit that charge separation between photogenerated holes and electrons is more efficient in NT_1 layers, in comparison with NT_2 and NT_3.

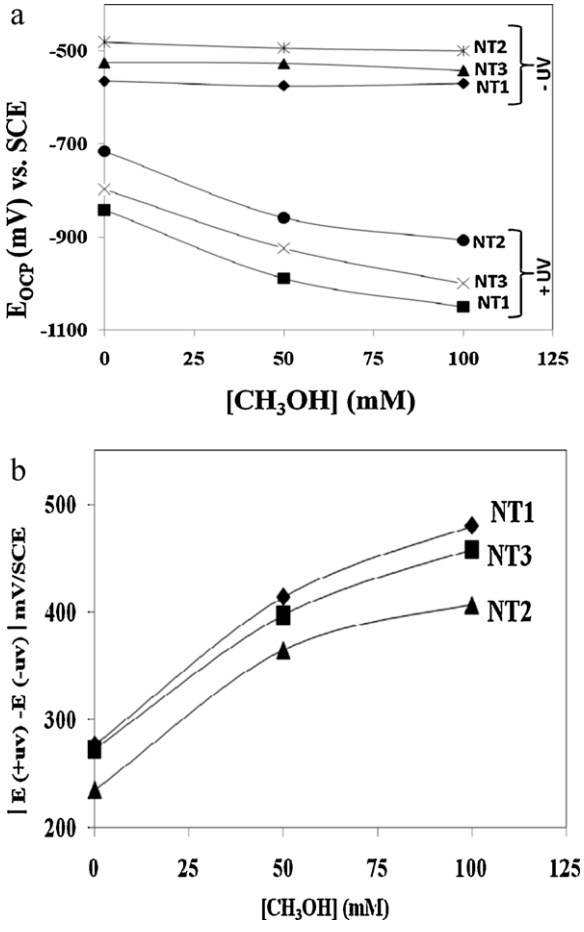

Fig. 3. (a) Open-circuit potential reached after 30 min in 0.1 mol/L NaOH as a function of methanol concentration, in the dark (−UV) and under illumination (+UV), (b) ΔE vs. methanol concentration.

3.5. Photocurrent measurements

Photocurrent measurements were carried out at 0.8 V, in a potential range where saturation of the photocurrent was reached and charge recombination in the semiconductor could be neglected. In these conditions the photocurrent I_{photo} can be estimated from empirical relation (4).

$$I_{photo} = K S_{spec} S_{\%} L\alpha \quad (4)$$

where α is the effective absorption coefficient for the spectral range of illumination, $\alpha = 0.5\ \mu m^{-1}$ in anatase [5]. S_{spec}, L and $S_{\%}$ values were defined above and are reported in Table 1.

K depends on the incident photon flux Φ_0 and on the coverage rate θ of reacting species at the surface of the nanotubes according to Eq. (5):

$$K = q\Phi_0\theta \quad (5)$$

It has dimension of a current density (A cm^{-2}) with q, the elementary charge.

Fig. 4 shows that the photocurrent for NT_1 is always higher than those of NT_2 and NT_3 samples, in the absence and in the presence of methanol. In absence of methanol, the reacting species are mainly adsorbed OH^-.

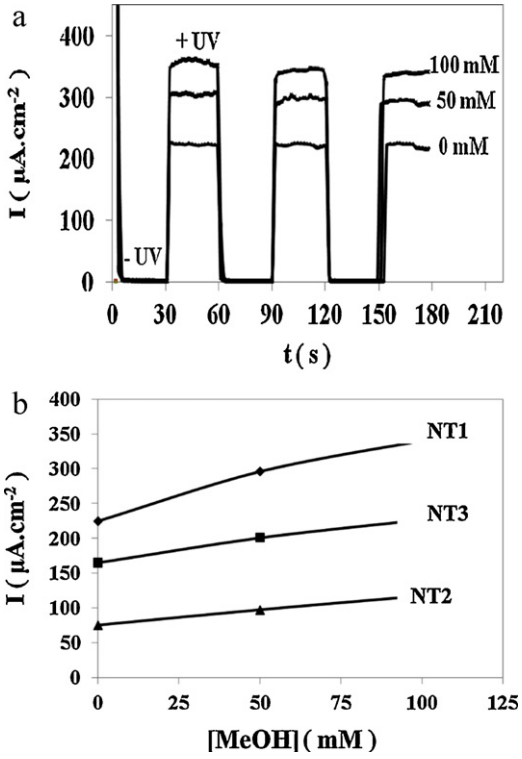

Fig. 4. (a) Photocurrent–time characteristics at 0.8 V/SCE for NT_1 sample; (b) photocurrent vs. methanol concentrations for the three nanotubular samples.

Table 2
Comparison between experimental and calculated photocurrent values on the bases of geometric characteristics of the NT layers.

Electrode	*I* photo (μA) experimental	$L\alpha$ (α = 5000 cm^{-1})	S_{spec} $S_{\%}$ $L\alpha$	*I* photo (μA) calculated
NT_1	230	0.62	8.7	230
NT_2	70	0.40	4.1	108
NT_3	160	0.87	5.8	153

Under a constant light intensity, and for a given concentration in reacting species, *K* remains constant. According to Eq. (4), in the absence of methanol, the photocurrents for NT_2 and NT_3 were calculated, extracting *K* from the experimental photocurrent measured for NT_1. The experimental and calculated values are compared in Table 2 and it appears that the differences between the measured photocurrent values can be attributed to differences in the geometric characteristics of the layer.

As shown in Fig. 4(a and b), the photocurrent responses also depend on methanol concentration. In Fig. 4(a), reported for NT_1 as an example, the rise and fall of the photocurrent at 0.8 V correspond well to the switch on and off of illumination. The variation of the photocurrent at this applied bias, as a function of methanol concentration is reported in Fig. 4(b), for the three types of electrodes. The observed increase of I_{photo} with methanol concentration is in good agreement with the results of Zhang et al. [37] showing a linear dependence of the saturation photocurrent with methanol concentration in the range of 0–100 mmol L^{-1}. They suggest that the steady-state photocurrent is first order with respect to methanol concentration in this low concentration range, and is limited by the light intensity at higher concentrations. An increase with methanol concentration of the oxidation rate by photogenerated holes is also in agreement with the shift of the open-circuit potential under lightening when the methanol concentration is increased.

3.6. Voltammetry

Under cathodic polarization, in aerated solutions several features can be observed for titanium oxide: besides expected oxygen and water reduction, a cation in-diffusion reaction, combined with reduction of the oxide, occurs simultaneously [38,39]. This later process is often electrochemically reversible and was reported to modify the electronic properties of the layer and to generate additional energy states within the band gap [30].

Fig. 5(a) shows a $i = f(E)$ curve performed in air-saturated 0.1 M NaOH solution, in the dark, starting from open-circuit potential (about −0.5 V) towards −2 V, followed by a reverse scan in the anodic range. A current plateau due to oxygen reduction is observed between −1 V and −1.5 V. At more negative potentials hydrogen evolution occurs. No specific feature for proton in-diffusion or oxide reduction can be distinguished, thus if they occur the corresponding current is included in the total cathodic current.

During the reverse scan, a current peak at −1.5 V is observed for the three layers but with different amplitudes.

3.6.1. Cathodic behaviour

We mainly focused on the current plateau due to oxygen reduction. The cathodic reduction of oxygen in the dark has been investigated by the past at several types of compact titanium oxide cathodes. In all cases, it was assumed to occur in alkaline solutions by a 4 electron-reaction into water [40]. Moreover it has been reported to occur through some active sites at the surface. According to Baez et al. [41], oxygen reduction is initiated by the surface reaction:

$$Ti(IV) + e^- \rightarrow Ti(III) \quad (6)$$

followed by an electron transfer from Ti(III) to oxygen.

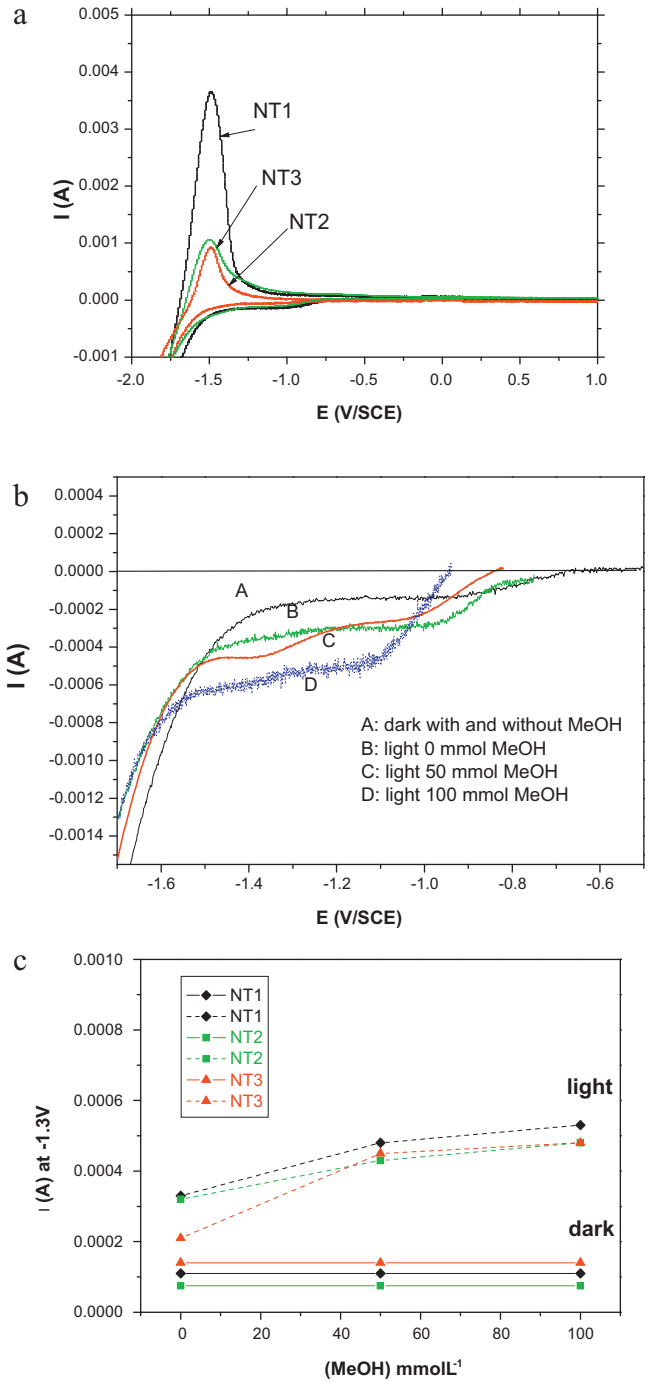

Fig. 5. Voltammogram (v = 50 mV/s) in 0.1 M MeOH: (a) for the 3 layers in the cathodic and anodic potential range; (b) for NT_1 in the cathodic potential range in the dark and under lightening; (c) evolution of the cathodic current measured at −1.3 V as a function of [MeOH].

Since oxygen reduction proceeds through the interaction of oxygen with Ti(III), the current for oxygen reduction is likely to be an indication of the amount of Ti(III) sites present in the three types of layers.

Ti(III) sites are produced on a cathodically polarized TiO_2 surface, but have also been shown to be photogenerated under band-gap illumination [30].

As an example, Fig. 5(b) shows the evolution of the current plateau for oxygen reduction in the case of NT1. In the dark, the current value (about 1.4×10^{-4} A) does not depend on the concentration of methanol. On the contrary, under illumination, the current plateau significantly increases and still increases when methanol concentration increases. Similar experiments were performed in the cases of NT_2 and NT_3, and the results are reported in Fig. 5(c). The 3 layers have similar behaviours.

Since TiO_2 is an n-type semiconductor the photo-induced cathodic current is not a real photocurrent. But if we assume that additional surface states like Ti(III) sites are generated during illumination at open-circuit potential, the increase of the cathodic current is correlated with these additional states. In the dark, the reduction current plateaus for oxygen are very close (75–140 μA), and the small differences can be due to slightly different active surfaces. Moreover in the dark, the reduction rate is independent of methanol concentration. Taking into account the geometric surface of the electrodes (0.64 cm^2), it is noticeable that a current density close to 2×10^{-4} A cm^{-2} is also usually measured for compact TiO_2 layers in the same conditions (here not shown). Consequently in the dark, the walls of the nanotubes are not likely to participate in the oxygen reduction reaction, and only the tube bottoms are likely to be active.

Under light exposure, in absence of methanol: Under lightening, the current increases for the three layers by a factor of 3, 4 and 2 for respectively NT_1, NT_2 and NT_3. If we assume that the current increase is due to activation of the wall surface, NT_1 should show the higher increase due to its higher specific surface (Table 1). Experimentally, this is not the case, since the cathodic current increase is more important for NT_2, in comparison with NT_1 and NT_3. This apparent contradiction suggests that during light exposure, more photoinduced surface states for electron storage are generated at the walls of the NT_2 layer, giving rise to new states available for oxygen reduction.

Under light exposure, in presence of methanol: The dependence of the cathodic current on methanol concentration is similar for the three types of layers and as previously can be attributed to the hole scavenging role of methanol, which hinders electron–hole recombination at open-circuit potential and allows more photoelectrons to be available for the generation of states at the wall surfaces.

3.6.2. Anodic behaviour

The peak appearing at −1.5 V during the reverse potential sweep has often been observed in the literature and has generally been attributed to the reverse of some reactions induced during the cathodic scan, such as oxidation of Ti (III) to the Ti (IV) [38,42] or de-insertion of protons. These two reactions involve energy states in the oxide layer and the surface of the peak is thus an indication of the presence of such states and of the reversibility of the charging–discharging reaction. Quantitative exploitation of this peak can here hardly be done, because the different events are difficult to be separated.

3.7. Electrochemical impedance spectrometry

Impedance spectroscopy has been shown to be an effective tool for in situ investigation of charge layer capacitance and accumulation properties in titanium oxide layers [11,12,14,15,23,30,31].

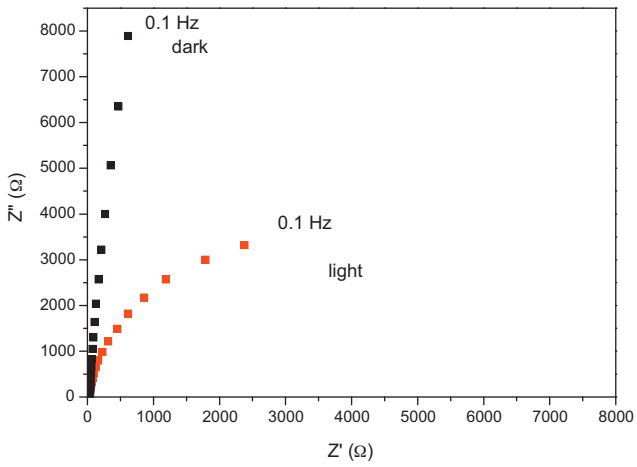

Fig. 6. Impedance diagrams in Nyquist representation for NT_1 nanotubular layer in supporting electrolyte (0.1 mol/L of NaOH) in the dark and under illumination.

Fig. 6 shows impedance diagrams in Nyquist representation for NT_1 samples, in the dark and under illumination, in absence of methanol in the electrolyte. In the dark, the behaviour is mainly capacitive, whereas under illumination an additional step due to charge transfer between TiO_2 and the electrolyte has to be taken into account. A contribution related to the response of energy traps in the nanostructured layer can generate an additional time constant, but its influence on impedance measurements is generally observed in a more anodic potential range [30].

3.7.1. In the dark

In the dark where no charge transfer is expected, the behaviour of the oxide layers can be well represented with two RC circuits connected in series [12] or in parallel [14,15]. The first RC circuit accounts for the behaviour of the space charge layer of the semiconducting oxide, whereas the second RC circuit describes relaxation via surface states. In the present work, the equivalent circuit used in order to characterize the electrochemical behaviour of the two layers is reported in Fig. 7(a). A (R_{SS}, C_{SS}, W_{SS}) series circuit corresponding to surface states is added in parallel to a basic R_T–CPE

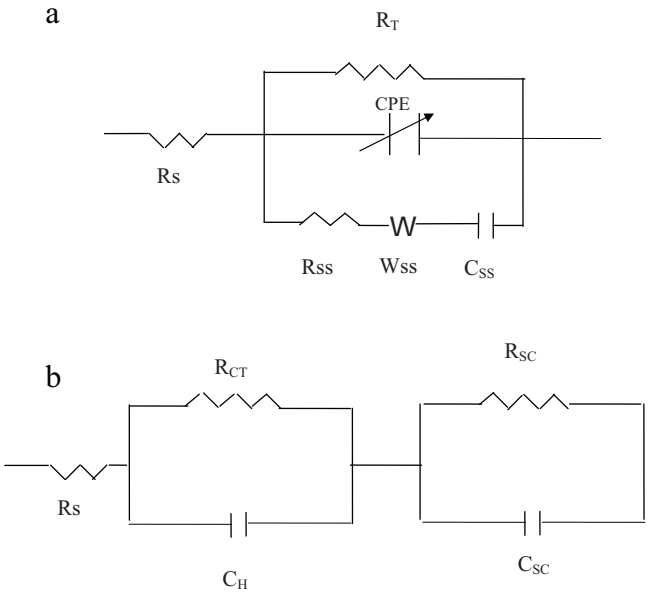

Fig. 7. Equivalent circuits used for impedance diagrams: (a) in the dark; (b) under lightening.

Table 3
Capacitance values Csc and C_{SS} extracted from impedance diagrams for the three layers in the dark.

Electrode/dark	[MeOH] mmol L^{-1}	$Q_0/\mu(\Omega^{-1}\ s^n)$	n	$C_{SC}/(\mu F)$ calculated from (7)	$C_{SS}/\mu F$
NT_1	0	47	1	47	145
NT_1	50	37	1	37	164
NT_1	100	38	1	38	161
NT_2	0	21	0.94	20	100
NT_2	50	39	0.95	28	86
NT_2	100	35	0.95	25	137
NT_3	0	34	0.96	25	136
NT_3	50	23	0.95	16	145
NT_3	100	38	1	38	154

circuit, and the result in series with an electrolyte resistance R_S. This model enables data fitting with a relative error for real and imaginary parts of the impedance of less than 1% over the whole frequency range. For the space charge layer of the semiconductor, a constant phase element (CPE) was used instead of a pure capacitance, though the exponent of the CPE was between 1 and 0.95 (Table 3), indicating a near ideal capacitive behaviour. R_{SS} and C_{SS} are associated respectively with surface states resistance and capacitance. The Warburg element W_{SS} is added to obtain a better fit and accounts for some delay in the surface states response. The true charge layer capacitance value C_{SC} was calculated using the following equation from Brug and co-workers [43]:

$$C = \frac{(RQ_0)^{1/n}}{R} \quad \text{where } R \text{ is defined by } \frac{1}{R} = \frac{1}{R_S} + \frac{1}{R_T} \tag{7}$$

where Q_0 is the constant representative for CPE ($\Omega^{-1}\ s^n$), n its exponent.

Impedance measurements were performed at the open-circuit potential for the three layers in the dark, as a function of methanol concentration and the values of the capacitance C_{SC} and C_{SS} are reported in Table 3.

It appears that space charge layer capacitance values vary between 16 and 47 μF for the three samples and do not depend on methanol concentration. This is in agreement with the conclusion from open-circuit potential measurements in the dark which showed that the values are very close for the three types of layer with and without methanol in the electrolyte (Fig. 3).

Surface state capacitance C_{SS} between 140 and 160 μF for NT_1, and NT_3, is slightly lower (between 80 and 140 μF) for NT_2 but keeps the same order of magnitude for the 3 methanol concentrations. It is noticeable that a Randle circuit with a simple R_P–CPE circuit in series with the electrolyte resistance can also be used, yet with a slightly higher fitting error. In the latter case, the equivalent capacitance is close to the sum of the parallel capacitances C_{SC} and C_{SS}.

3.7.2. Under illumination

As shown in Fig. 3, in passing from dark to illumination the open-circuit potential reaches a very negative value which is then close to the conduction band. The equivalent circuit used in this case is reported in Fig. 7(b). A (R_{CT}, C_H,) circuit corresponding to charge transfer (R_{CT} is the charge transfer resistance and C_H is the capacitance of the Helmholtz layer) is added in series with a R_{SC}–C_{SC} circuit, and the result in series with an electrolyte resistance R_S. This model enables data fitting with a relative error for real and imaginary parts of the impedance of less than 2% over the whole frequency range. For the semiconductor, the capacitance C_{sc} includes the space charge layer and the surface states capacitance. Since in the potential range close to the conduction band most energy states in the gap are filled with photogenerated electrons, the C_{sc} value can be considered to be mainly due to the space charge layer. C_H, C_{SC} and R_{CT} values during light exposure are reported in Table 4 as a function of methanol concentration, for the 3 types of nanotubular layers.

The R_{CT} values have the same order of magnitude for the three types of layers. The decrease of R_{CT} when methanol concentration increases is correlated with an increase of the rate of charge transfer as expected.

In passing from dark to illumination an increase of C_{SC} is observed which is similar for NT_1, NT_2 and NT_3. This is partly due to the shift of the open-circuit potential towards more cathodic, but can also be attributed to the increase of the active surface since UV excitation of the nanotubes induces activation of the tube walls [30]. A noticeable result is the increase of the semiconductor capacitance with methanol concentration, which can also be correlated to the higher photopotential in presence of higher concentrations of MeOH (Fig. 3). This effect was attributed above to the fact that a higher methanol concentration and consequently a higher amount of adsorbed methanol at the surface of the tubes allows more electrons to accumulate in the electrode, generating Ti(III) species as surface states.

Another noticeable result is the huge value of the double layer capacitance, which, in aqueous solutions, is usually close to 50 μF/cm^2. That clearly shows that the whole surface, including the tube walls, is active. In Table 4, if the extracted C_H values are divided by the specific surface reported in Table 1, values of double layer capacitance between 28 and 85 μF/cm^2 are determined. This is an additional proof that the whole surface of the tubes is activated during lightening.

The C_{SC} values divided by the specific surface of each layer are also reported in Table 4. It appears that NT_2 shows the higher capacitance density, yet the lower photopotential (Fig. 3). As stated previously, if we assume that C_{SC} involves simultaneously the charge layer capacitance and the surface state capacitance, the high value under illumination of C_{SC} in the case of NT_2 is likely to be due to the generation of a higher amount of surface states in comparison with NT_1 and NT_3. This is in agreement with the observations made during cathodic reduction of oxygen via surface states (see Section 3.6.1).

3.8. Photocatalytic (PC) degradation of AB

In order to compare the photocatalytic efficiency of the three nanotubular TiO_2 electrodes, the variation of relative concentration of Amino Black (AB) as a function of reaction time was carried out and shown in Fig. 8(a).

It was observed that the degradation of dye proceeded much faster in the presence of NT_1 as compared with the two others TiO_2 nanotubes samples. Fig. 8(b) shows that a 96.6% decolouration efficiency of dye in aqueous solution was achieved after 45 min of reaction using NT_1, while the decolourization efficiencies obtained for NT_2 and NT_3 were only 73.5 and 80.0%, respectively, within the same time. It is noticeable that the degradation rate measured on a TiO_2 compact layer (not shown here) in the same experimental

Table 4
Capacitance C_H and C_{SC}, and charge transfer resistance values extracted from impedance diagrams for the three layers under lightening.

Electrode/light exposure	[MeOH] (mmol L^{-1})	C_H (μF)	C_H/S_{spec} (μF/cm^2)	R_{CT} (Ω)	C_{SC} (μF)	C_{SC}/S_{spec} (μF/cm^2)
NT_1	0	1970	50	20	315	8.1
NT_1	50	1973	50	18	325	8.3
NT_1	100	1104	28	4	676	17.3
NT_2	0	1961	85	13	301	13
NT_2	50	1160	50	11	330	14.3
NT_2	100	1078	47	4	591	26.7
NT_3	0	1667	57	37	259	8.9
NT_3	50	883	30	5	380	13.1
NT_3	100	1083	36	4	620	21.3

conditions lead to an efficiency of only 17% after 45 min of treatment.

The reason often put forward to explain the good photocatalytic behaviour of NT layers is the large surface area, which provides high contact area for absorption of dye or pollutants. In the present work, the solid fraction depending on the voids between the tubes and the thickness of the tube walls was also taken into account to estimate the level of excitation in the oxide layer. Photocurrent measurements in the saturation range clearly showed that the difference in efficiency between the three types of layers can be attributed to their differences in morphology: specific surface but also solid fraction available for generated charges (Tables 1 and 2). Since the photocatalytic performances are correlated with the photocurrent,

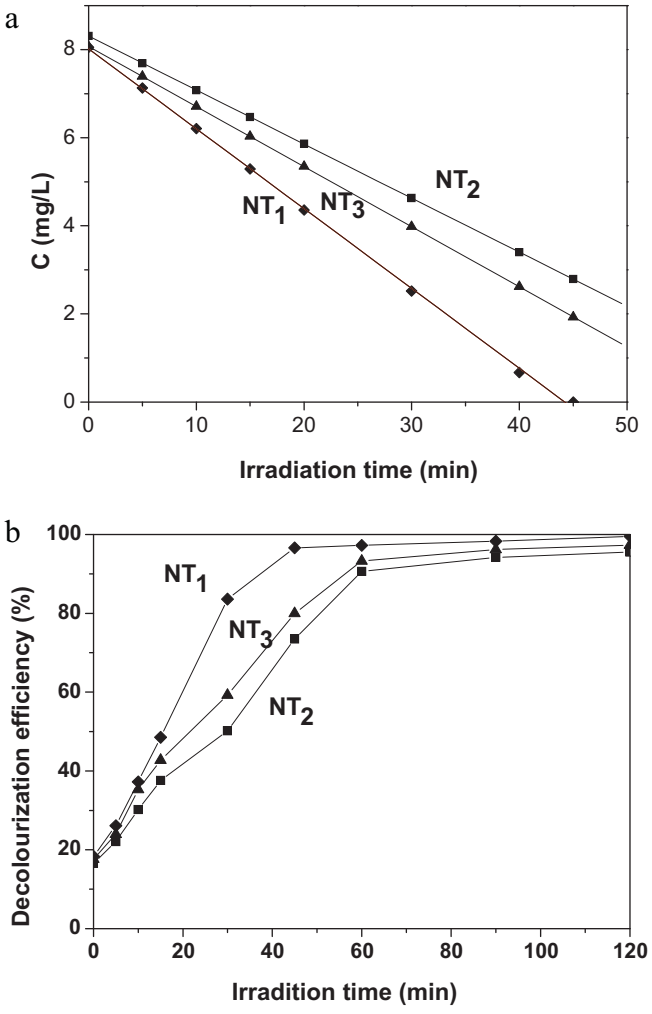

Fig. 8. (a) PC degradation of black amido (Co = 10 mg/L, λ = 618 μm); (b) decolourization efficiency of Black Amido.

the comparison between NT_1, NT_2, NT_3 leads to attribute the higher photocatalytic efficiency in NT_1 to a higher (S_{spec} $S_{\%}$ $L\alpha$) product under UV light. Since the tube wall thickness is similar for the three types of layers, the influence of this parameter on the photocatalytic performances cannot be confirmed in the present work, as was suggested in Ref. [28].

In passing from dark to light exposure, potentiodynamic measurements in the cathodic potential range evidenced the higher increase in the rate of oxygen reduction for NT_2 in comparison with NT_2 and NT_3, due to a higher amount of photo-generated surface states. Accordingly, impedance measurements performed at open-circuit potential showed a higher capacitance increase for the NT_2 layer under light exposure. From these results it seems that the photo-catalytic performances of a NT layer are mainly determined by the specific surface and the solid fraction of the layer in which photo-charges are created. They are not influenced by the photo-generated surface states in which photoelectrons can be stored.

4. Conclusion

The nanotubular TiO_2 electrodes were obtained by anodization of a Ti sheet at 20 V for 45 min in three different media. The three types of layers showed similar thickness (between 800 and 1700 nm) and the tube-walls had the same thickness (between 15 and 20 nm). The titania nanotube electrode prepared in ethylene glycol (NT_1) showed a higher photocurrent, and a higher activity for pollutant degradation. This result is attributed to a good compromise between a high specific surface and the higher solid fraction able to absorb incident photons to convert into hole–electron pairs.

If we consider the amount of photo-generated traps in the tube walls, it appears that in passing from dark to UV exposure, the NT_2 layer characterized by rough walls, exhibits the higher increase in surface state generation, and this result is also confirmed through impedance measurements, by a higher capacitance density increase under light exposure. From these first results, it seems that photo-generated surface states have no influence on the photocatalytic activity of a nanotubular layer. The main raison is that photo-generated surface states able to trap photoelectrons are different from the states at which holes can recombine or through which they are transferred to the electrolyte. But further experiments are required to confirm this assumption.

Acknowledgement

The authors wish to thank Stephan Borensztajn (CNRS, UPR15-LISE) for SEM pictures.

References

[1] M.R. Hoffman, S.T. Martin, W. Choi, D.W. Bahnemann, Environmental applications of semiconductor photocatalysis, Chem. Rev. 95 (1995) 69–96.
[2] C. Ruan, M. Paulose, O.K. Varghese, G.K. Mor, C.A. Crimes, Fabrication of highly ordered TiO_2 nanotube arrays using an organic electrolyte, J. Phys. Chem. B 109 (2005) 15754–15759.

[3] N. Wang, X. Li, Y. Wang, X. Quan, G. Chen, Evaluation of bias potential enhanced photocatalytic degradation of 4-chlorophenol with TiO_2 nanotube fabricated by anodic oxidation method, Chem. Eng. J. 146 (2009) 30–35.
[4] Y.F. Tu, S.Y. Huang, J.P. Sang, X.W. Zou, Synthesis and photocatalytic properties of Sn-doped TiO_2 nanotube arrays, J. Alloys Compd. 482 (2009) 382–387.
[5] R.P. Lynch, A. Ghicov, P. Schmuki, A photo-electrochemical investigation of self-organized TiO_2 nanotubes, J. Electrochem. Soc. 157 (2010) G76–G84.
[6] G.K. Mor, K. Shankar, M. Paulose, O.K. Varghese, C.A. Grimes, Use of highly-ordered TiO_2 nanotube arrays in dye-sensitized solar cells, Nano Lett. 6 (2006) 215–218.
[7] K. Zhu, N.R. Neale, A. Miedaner, A.J. Frank, Enhanced charge-collection efficiencies and light scattering in dye-sensitized solar cells using oriented TiO_2 nanotubes arrays, Nano Lett. 7 (2007) 69–74.
[8] K. Zhu, T.B. Vinzant, N.R. Neale, A.J. Frank, removing structural disorder from oriented TiO_2 nanotubes arrays: reducing the dimensionality of transport and recombination in dye-sensitized solar cells, Nano Lett. 7 (2007) 3739–3746.
[9] F. Fabregat-Santiago, I. Mora-Sero, G. Garcia-Belmonte, J. Bisquert, Cyclic voltammetry studies of nanoporous semiconductors. Capacitive and reactive properties of nanocrystalline TiO_2 electrodes in aqueous electrolyte, J. Phys. Chem. B 107 (2003) 758–768.
[10] J. Nelson, Continuous-time random-walk model of electron transport in nanocrystalline TiO_2 electrodes, Phys. Rev. B 59 (1999) 15374–15380.
[11] W.H. Leng, Z. Zhang, J.Q. Zhang, C.N. Cao, Investigation of the kinetics of a TiO_2 Photoelectrocatalytic reaction involving charge transfer and recombination through surface states by electrochemical impedance spectroscopy, J. Phys. Chem. B 109 (2005) 15008–15023.
[12] A.G. Munoz, Semiconducting properties of self-organized TiO_2 nanotubes, Electrochim. Acta 52 (2007) 4167–4176.
[13] T. Berger, T. Lana-Villarreal, D. Monllor-Satoca, R. Gomez, An electrochemical study on the nature of trap states in nanocrystalline rutile thin films, J. Phys. Chem. C 111 (2007) 9936–9942.
[14] V. Spagnol, E. Sutter, C. Debiemme-Chouvy, H. Cachet, B. Baroux, EIS study of photo-induced modifications of nano-columnar TiO_2 films, Electrochim. Acta 54 (2009) 1228–1232.
[15] V. Spagnol, H. Cachet, B. Baroux, E. Sutter, Influence of sub-band-gap states on light induced log-lasting super-hydrophilic behaviour of TiO_2, J. Phys. Chem. C 113 (2009) 3793–3799.
[16] H. Wang, J. He, G. Boschloo, H. Lindström, A. Hagfeldt, S.T. Lindquist, Electrochemical investigation of traps in a nanostructured TiO_2 film, J. Phys. Chem. B 105 (2001) 2529–2533.
[17] T. Berger, M. Sterrer, O. Diwald, E. Knözinger, D. Panayotov, T.L. Thompson, J.T. Yates, Light-induced charge separation in anatase TiO_2 particles, J. Phys. Chem. B 109 (2005) 6061–6068.
[18] S.A. Haque, Y. Tachibana, R.L. Willis, J.E. Moser, M. Grätzel, D.R. Klug, J.R. Durrant, Parameters influencing charge recombination kinetics in dye-sensitized nanocrystalline titanium dioxide films, J. Phys. Chem. B 104 (2000) 538–547.
[19] G.K. Mor, O.K. Varghese, M. Paulose, K. Shankar, C.A. Grimes, A review on highly ordered, vertically oriented TiO_2 nanotube arrays: fabrication, material properties, and solar energy applications, Sol. Energy Mater. Sol. Cells 90 (2006) 2011–2075.
[20] J.M. Macak, H. Tsuchiya, A. Ghicov, K. Yasuda, R. Hahn, S. Bauer, P. Schmuki, TiO_2 nanotubes: self-organized electrochemical formation, properties and applications, Curr. Opin. Solid State Mater. Sci. 11 (2007) 3–18.
[21] C. Ruan, M. Paulose, O.K. Varghese, C.A. Grimes, Enhanced photoelectrochemical-response in highly ordered TiO_2 nanotube-arrays anodized in boric acid containing electrolyte, Sol. Energy Mater. Sol. Cells 90 (2006) 1283–1295.
[22] H. Tsuchiya, J.M. Macak, L. Taveira, E. Balaur, A. Ghicov, K. Sirotna, P. Schmuki, Self-organized TiO_2 nanotubes prepared in ammonium fluoride containing acetic acid electrolytes, Electrochem. Commun. 7 (2005) 576–580.
[23] L. Taveira, A. Sagüés, J.M. Macak, P. Schmuki, Impedance behavior of TiO_2 nanotubes formed by anodization in NAF electrolytes, J. Electrochem. Soc. 155 (2008) C293–C302.
[24] S. Li, G. Zhang, D. Guo, L. Yu, W. Zhang, Anodization fabrication of highly ordered TiO_2 nanotubes, J. Phys. Chem. C 113 (2009) 12759–12765.
[25] J. Yu, B. Wang, Effect of calcinations temperature on morphology and photoelctrochemical properties of anodized titanium dioxide nanotube arrays, Appl. Catal. B 94 (2010) 295–302.
[26] J. Yu, G. Dai, B. Cheng, Effect of crystallization methods on morphology and photocatalytic activity of anodized TiO_2 nanotube array films, J. Phys. Chem. C 114 (2010) 19378–19385.
[27] G. Dai, J. Yu, G. Liu, Synthesis and enhanced visible-light photoelectrocatalytic activity of p–n junction BiOI/TiO_2 nanotube arrays, J. Phys. Chem. C 115 (2011) 7339–7346.
[28] M. Zlamal, J.M. Macak, P. Schmuki, J. Krysa, Electrochemically assisted photocatalysis on self-organized TiO_2 nanotubes, Electrochem. Commun. 9 (2007) 2822–2826.
[29] H.E. Prakasam, K. Shankar, M. Paulose, O.K. Varghese, C.A. Grimes, A new benchmark for TiO_2 nanotube array growth by anodization, J. Phys. Chem. C 111 (2007) 7235–7241.
[30] P. Pu, H. Cachet, E.M.M. Sutter, Electrochemical impedance spectroscopy to study photo-induced defects on self-organized TiO_2 nanotube arrays, Electrochim. Acta 55 (2010) 5938–5946.
[31] F. Fabregat-Santiago, E.M. Barea, J. Bisquert, G.K. Mor, K. Shankar, C.A. Grimes, High carrier density and capacitance in TiO_2 nanotube arrays induced by electrochemical doping, J. Am. Chem. Soc. 130 (2008) 11312–11316.
[32] S. Sreekantan, L.M. Hung, Effects of electrolyte natures on the formation of well-ordered titania nanotubes produced via anodisation, J. Phys. Sci. 20 (2009) 61–71.
[33] K. Yanagisawa, J. Ovenstone, Crystallization of anatase from amorphous titania using the hydrothermal technique: effects of starting material and temperature, J. Phys. Chem. B 103 (1999) 7781–7787.
[34] K.L. Frindell, M.H. Bartl, A. Popitsch, G.D. Stucky, Sensitized luminescence of trivalent europium by three-dimensionally arranged anatase nanocrystals in mesostructured titania thin films, Angew. Chem. Int. Ed. 41 (2002) 959–962.
[35] M.P. Moret, R. Zallen, D.P. Vijay, S.B. Desu, Brookite-rich titania films made by pulsed laser deposition, Thin Solid Films 366 (2000) 8–10.
[36] A.G. Kontos, A.I. Kontos, D.S. Tsoukleris, V. Likodimos, J. Kunze, P. Schmuki, P. Falaras, Photo-induced effects on self-organized TiO_2 nanotube arrays: the influence of surface morphology, Nanotechnology 20 (2009), 045603 1-9.
[37] Z. Zhang, Y. Yuan, Y. Fang, L. Liang, H. Ding, G. Shi, L. Jin, Photoelectrochemical oxidation behaviour of methanol on highly ordered TiO_2 nanotube array electrodes, J. Electroanal. Chem. 610 (2007) 179–185.
[38] A. Ghicov, H. Tsuchiya, R. Hahn, J.M. Macak, A.G. Munoz, P. Scmuki, TiO_2 nanotubes: H^+ insertion and strong electrochromic effects, Electrochem. Commun. 8 (2006) 528–532.
[39] H. Pelouchova, P. Janda, J. Weber, L. Kavan, Charge transfer reductive doping of single crystal TiO_2 anatase, J. Electroanal. Chem. 566 (2004) 73–83.
[40] S.V. Mentus, Oxygen reduction on anodically formed titanium dioxide, Electrochim. Acta 50 (2004) 27–32.
[41] V.B. Baez, J.E. Graves, D. Pletcher, The reduction of oxygen on titanium dioxide electrodes, J. Electroanal. Chem. 340 (1992) 273–286.
[42] G. Boschloo, D. Fitzmaurice, Electron accumulation in nanostructured TiO_2 (anatase) electrodes, J. Electrochem. Soc. 147 (2000) 1117–1123.
[43] G.J. Brug, A.L.G. van den Eeden, M. Sluyters-Rehbach, J.H. Sluyters, The analysis of electrode impedances complicated by the presence of a constant phase element, J. Electroanal. Chem. 176 (1984) 275–295.